

The physical parameters of Markarian 501 during flaring activity

W. Bednarek^{1,2} and R.J. Protheroe¹

¹Department of Physics and Mathematical Physics
The University of Adelaide, Adelaide, Australia 5005.
rprother@physics.adelaide.edu.au

²University of Łódź, 90-236 Łódź, ul. Pomorska 149/153, Poland.
bednar@krysia.uni.lodz.pl

Abstract

We determine the physical parameters (magnetic field and Doppler factor) of the homogeneous synchrotron self-Compton model allowed by the observed X-ray to gamma-ray spectra and variability of Markarian 501 during the 15–16 April 1997 flaring activity. We find that magnetic fields between 0.07 G and 0.6 G and Doppler factors between 12 and 36 could fit (depending on observed variability time scale) these observations. We take account of photon-photon pair production interactions of gamma-ray photons occurring both inside the emission region and during propagation to Earth and find these to be extremely important in correctly determining the allowed model parameters. Previous estimates of the allowed parameter space have neglected this effect. Future multi-wavelength campaigns during strong flaring activity, including observations from optical to TeV gamma-rays, should enable the physical parameters to be further constrained.

keywords: galaxies: active – quasars: jets – radiation mechanisms: gamma rays – galaxies: individual: Mrk 501

1 Introduction

Four BL Lac objects have been detected in the TeV energy range: Mrk 421 (Punch et al. 1992), Mrk 501 (Quinn et al. 1996), 1E S2344+514 (Catanese et al. 1998), and PKS 2155-304 (Chadwick et al. 1998). In two of these, Mrk 421 and Mrk 501, the high level of γ -ray emission enabled the spectrum to be measured up to ~ 10 TeV (Zweerink et al. 1997,

Aharonian et al. 1997, Samuelson et al. 1998, Djannati-Atai et al. 1998, Hayashida et al. 1998). In the case of Mrk 421, the spectrum can be adequately described by a single power law between 0.3 - 10 TeV. However the spectrum of Mrk 501 shows clear curvature over a similar energy range (Krennrich 1998). Recently, the spectrum of Mrk 501 has been measured up to 24 TeV by the HEGRA telescopes (Konopelko et al. 1999, Krawczynski et al. 1999).

The γ -ray emission of these two BL Lacs shows very rapid variability. For Mrk 421, variability on a time scale as short as ~ 15 minutes has been reported (Gaidos et al. 1996). In the case of Mrk 501, variability on a time scale of a few hours was observed during the 1997 high level of activity (Aharonian et al. 1998, Quinn et al. 1999 cited by Krennrich et al. 1998), and there is some evidence of variability on a time scale of 20 minutes (Aharonian et al. 1998).

The TeV γ -ray flares are simultaneous with the X-ray flares. In the case of Mrk 501, during the 16 April 1997 flare the X-ray spectrum was observed by the Beppo-SAX observatory up to ~ 200 keV (Pian et al. 1998), and during the same high state OSSE observations made between 9 to 15 April 1997 (Catanese et al. 1997) show that the energy flux per log energy interval continues up to ~ 500 keV at roughly the same level.

Gamma-ray emission from active galactic nuclei (AGN) is often interpreted in terms of the homogeneous “synchrotron self-Compton model” (SSC) in which the low energy emission (from radio to X-rays) is synchrotron radiation produced by electrons which also up-scatter these low energy photons into high energy γ -rays by inverse Compton scattering (ICS) (Macomb et al. 1995, Inoue & Takahara 1996, Bloom & Marscher 1996, Mastichiadis & Kirk 1997). In this model all the radiation comes from this same region in the jet. Such a picture can naturally explain synchronized variability at different photon energies.

The inclusion of photon-photon pair production interactions of γ -rays with low energy radiation within the emission region has been used previously when constraining the physical parameters of blazars (e.g. Mattox et al. 1993, Dondi & Ghisellini 1995). This was also included in our previous paper (Bednarek and Protheroe 1997) where we constrained the allowed parameter space of the homogeneous SSC model, i.e. the magnetic field in the emission region and the Doppler factor, based on observations of the 1994 flaring activity in Mrk 421. More recently, a similar analysis has been performed for Mrk 501 by various authors (Kataoka et al. 1999, Tavecchio, Maraschi and Ghisellini 1998). However, in this recent work absorption on both the infrared background (IRB) and the internal radiation of the emission region has been neglected. In the present paper we show that inclusion of both these effects is vital in order to properly determine the allowed parameter space.

In Section 2 we discuss the effect of photon-photon pair production interactions of γ -rays with synchrotron radiation produced inside the emission region, and with IRB photons during propagation to Earth. In Section 3 we obtain the values of B and D allowed by the observed ratio of γ -ray to X-ray power, and in Section 4 we discuss additional constraints arising from the requirement that the radiative cooling time must be consistent with the observed variability time scale. In Section 5, we further narrow

down the allowed model parameters by comparing the predicted TeV γ -ray spectrum with that observed, and finally we discuss the implications of our results.

2 Absorption of Gamma-Rays by Photon Photon Pair Production

For propagation of γ -rays through isotropic radiation the reciprocal of the mean interaction length for photon-photon pair production is given by

$$x_{\gamma\gamma}(E_\gamma)^{-1} = \frac{1}{8E_\gamma^2} \int_{\varepsilon_{\min}}^{\infty} d\varepsilon \frac{n(\varepsilon)}{\varepsilon^2} \int_{s_{\min}}^{s_{\max}(\varepsilon, E_\gamma)} ds s \sigma(s), \quad (1)$$

where $n(\varepsilon)$ is the differential photon number density and $\sigma(s)$ is the total cross section for photon-photon pair production (Jauch and Rohrlich 1955) for a centre of momentum frame energy squared given by $s = 2\varepsilon E_\gamma(1 - \cos\theta)$ where θ is the angle between the directions of the energetic photon and soft photon, and $s_{\min} = (2m_e c^2)^2$, $\varepsilon_{\min} = (2m_e c^2)^2/4E_\gamma$, and $s_{\max}(\varepsilon, E_\gamma) = 4\varepsilon E_\gamma$.

We shall now apply these formulae directly to obtain the mean interaction length in the IRB and, in a modified form, to obtain the optical depth in the synchrotron radiation produced in the emission region.

2.1 Absorption of gamma-rays in the infrared background

The spectra of γ -rays from extragalactic objects are modified by photon photon pair production interactions with the infrared background, and observations of the γ -ray spectra of Mrk 421 and Mrk 501 have been used to constrain the intensity of the infrared background (Stanev and Franceschini 1998, Biller et al. 1998). Recently, Malkan and Stecker (1998) have modelled the infrared background by summing the contributions from different types of galaxy taking account of evolution. We use their upper and lower models which are consistent with recent COBE DIRBE data (Hauser et al. 1998) and COBE FIRAS data (Fixsen et al. 1998) which we use to extend the model of Malkan and Stecker down below $3 \mu\text{m}$.

We obtain the mean interaction length, $x_{\gamma\gamma}(E_\gamma)$, in the IRB plus cosmic microwave background radiation (CMBR) and these are shown in Fig. 1(a). We also show separately the mean free path in the CMBR alone. Our results are in good agreement with those of Stecker and De Jager (1998) calculated for the same infrared background models (see Stecker and De Jager for references to earlier work). In Fig. 1(b) we show the reduction factor, $R(E_\gamma) = \exp[-\tau_{\text{IR}}(E_\gamma)] \equiv \exp[-d/x_{\gamma\gamma}(E_\gamma)]$ for a source distance of $d = 202 \text{ Mpc}$ obtained for Mrk 501 assuming $H_0 = 50 \text{ km s}^{-1} \text{ Mpc}^{-1}$ and a redshift of $z = 0.033$. Clearly, absorption in the IR background becomes very important above 400 GeV. Figure 2 shows the 1997 April 15–16 HEGRA and CAT data together with the approximation used later in this paper for the high energy part of the spectral energy distribution (SED).

The figure also shows this SED after correction for absorption in the infrared using the two reduction factors of Fig. 1(b).

2.2 Absorption of gamma-rays in the blob radiation

Absorption of γ -rays will also take place on the synchrotron photons produced inside the emission region. For the spectrum of these target photons we use a fit to the Beppo-SAX observations made during the April 15/16 flaring activity (Pian et al. 1998), together with an indication from OSSE Observations made during the high state in April 1997 (Catanese et al. 1997) that the spectrum continued to $\varepsilon_{s,\max} = 500$ keV with approximately the same energy flux per log energy interval. The differential photon flux in the optical to X-ray region observed from Mrk 501 during the 16 April 1997 flare (photons $\text{cm}^{-2} \text{s}^{-1} \text{GeV}^{-1}$) is approximated by

$$F(\varepsilon) \approx \begin{cases} 3 \times 10^{-4} \varepsilon^{-1.4} & \varepsilon \leq \varepsilon_{s,1} = 2.14 \times 10^{-6} \text{GeV}, \\ 2.5 \times 10^{-5} \varepsilon^{-1.59} & \varepsilon_{s,1} < \varepsilon \leq \varepsilon_{s,2} = 1.95 \times 10^{-5} \text{GeV}, \\ 1.86 \times 10^{-6} \varepsilon^{-1.83} & \varepsilon_{s,2} < \varepsilon \leq \varepsilon_{s,3} = 2 \times 10^{-4} \text{GeV}, \\ 4.37 \times 10^{-7} \varepsilon^{-2} & \varepsilon_{s,3} < \varepsilon \leq \varepsilon_{s,\max}. \end{cases} \quad (2)$$

The photon density in the emission region depends on the dimensions of the source and the assumed Doppler factor. We assume that relativistic electrons are confined inside a “blob” which moves along the jet with the Doppler factor D and has magnetic field B . In the homogeneous SSC model the radii of the emission regions of low energy photons (r_l), X-ray photons (r_X), and TeV γ -rays (r_γ) are the same. This region is constrained by the variability time scale observed, e.g. in TeV γ -rays, t_{var} ,

$$r_l = r_\gamma = r_X \approx 0.5 \xi c D t_{\text{var}} \quad (3)$$

where $\xi \leq 1$, $\xi = 1$ being the usual assumption. The differential photon density in the blob frame of synchrotron photons is then given by

$$n(\varepsilon') \approx \frac{4d^2 F(\varepsilon)}{c^3 t_{\text{var}}^2 D^4 \xi^2}, \quad (4)$$

where $\varepsilon = D\varepsilon'$ and ε' are the photon energies in the observer’s and the blob rest frames, and c is the velocity of light.

The optical depth $\tau_{\text{syn}}(E'_\gamma)$ in the blob frame for γ -ray photons with blob-frame energy $E'_\gamma = E_\gamma/D$ for e^\pm pair production inside the blob is given by

$$\tau_{\text{syn}}(E'_\gamma) = \frac{r_\gamma}{8E'_\gamma{}^2} \int_{\varepsilon'_{\min}}^{\infty} d\varepsilon' \frac{n(\varepsilon')}{\varepsilon'^2} \int_{s_{\min}}^{s_{\max}(\varepsilon', E'_\gamma)} ds s \sigma(s). \quad (5)$$

We compute the optical depth by numerical integration of Eq. 5, and our results can be approximated very well in the energy range of interest, i.e. $0.1 \text{ TeV} < E_\gamma < 100 \text{ TeV}$, by

$$\tau_{\text{syn}}(E_\gamma) \approx 3 \times 10^8 D^{-4.8} E_\gamma^{0.4} t_{\text{var}}^{-1} \xi^{-1}, \quad (6)$$

for $1 \leq D \leq 100$ and $10^2 \text{ s} \leq t_{\text{var}} \leq 10^4 \text{ s}$. We note that the $E_\gamma^{0.4}$ energy dependence we obtain is consistent with equation (B7) of Svensson (1987) for a photon spectral index of 1.6. From Eq. 6, we find that $D \gg 13$ to avoid absorption at 1 TeV if the variability time is 20 minutes and applying $\xi = 1$. Clearly absorption by photon-photon interactions inside the blob can not be neglected.

3 Constraint from Ratio of Gamma-Ray to X-ray Power

The spectrum of Mrk 501 shows two clear bumps which, during the outburst stage, extend up to at least $\sim 500 \text{ keV}$ (Pian et al. 1998, Catanese et al. 1997), and up to at least $\sim 10 \text{ TeV}$ (Aharonian et al. 1997, Krennrich et al. 1999, Djannati-Atai et al. 1998, Hayashida et al. 1998, see also Protheroe et al. 1998 for review), the highest energy of γ -rays observed being 24 TeV (Konopelko et al. 1999, Krawczynski et al. 1999). These multiwavelength observations of Mrk 501 allow us to define the ratio η of the energy flux per log energy interval observed at a chosen γ -ray energy, $E_\gamma = 1 \text{ TeV}$, at which the emission is assumed to be due to Compton scattering, to that at a chosen X-ray energy, $\varepsilon = 2 \text{ keV}$, at which the emission is assumed to be due to synchrotron radiation,

$$\eta = \left(\frac{dN}{dE_\gamma dt} E_\gamma^2 e^{-\tau_{\text{tot}}(E_\gamma)} \right) / \left(\frac{dN}{d\varepsilon dt} \varepsilon^2 \right) = \left(\frac{dN}{dE'_\gamma dt'} E'^2_\gamma e^{-\tau_{\text{tot}}(E'_\gamma)} \right) / \left(\frac{dN}{d\varepsilon' dt'} \varepsilon'^2 \right), \quad (7)$$

where $\tau_{\text{tot}}(E_\gamma) = \tau_{\text{syn}}(E_\gamma) + \tau_{\text{IR}}(E_\gamma)$ is the total optical depth for photons in the synchrotron radiation of the blob and the infrared-microwave background, and the primed quantities are measured in the blob frame. For the power at γ -ray energies we adopt the value reported by the CAT experiment at $E_\gamma = 1 \text{ TeV}$ (Djannati-Atai et al. 1998), and for the power at X-ray synchrotron energies we take the value at $\varepsilon = 2 \text{ keV}$ (Pian et al. 1998). For these two energies $\eta \approx 3.6$, and from this constraint we shall now obtain the required magnetic field as a function of the Doppler factor for various variability time-scales.

The synchrotron spectrum at ε' in the above formula (Eq. 7) can be approximated analytically by

$$\varepsilon' \frac{dN}{d\varepsilon' dt} d\varepsilon' \approx \frac{dN}{d\gamma'} d\gamma' b_{\text{syn}}(\gamma'), \quad (8)$$

where $dN/d\gamma'$ is the electron spectrum in the blob rest frame. $b_{\text{syn}}(\gamma') = kU_B\gamma'^2$ is the energy loss rate of electrons, where $k = 4c\sigma_T/3$, σ_T is the Thomson cross section, and U_B is the magnetic field energy density. The characteristic energy of synchrotron photons is given by

$$\varepsilon' \approx 0.5\varepsilon_B\gamma'^2. \quad (9)$$

We use the observed low energy SED (Eq. 2) to estimate the blob-frame equilibrium electron spectrum

$$\frac{dN}{d\gamma'} \approx \begin{cases} a_1 \gamma'^{-1.8} & \gamma' \leq \gamma'_{b,1}, \\ a_2 \gamma'^{-2.18} & \gamma'_{b,1} < \gamma' \leq \gamma'_{b,2}, \\ a_3 \gamma'^{-2.66} & \gamma'_{b,2} < \gamma' \leq \gamma'_{b,3}, \\ a_4 \gamma'^{-3} & \gamma'_{b,3} < \gamma' \leq \gamma'_{b,\max}, \end{cases} \quad (10)$$

where γ' is the Lorentz factor in the blob frame,

$$\gamma'_{b,n} = (2\varepsilon_{b,n}/D\varepsilon_B)^{1/2}, \quad (11)$$

where $n = 1, 2, 3$, and $a_1 = \gamma'_{b,1}^{-0.38}$, $a_2 = 1$, $a_3 = \gamma'_{b,2}^{0.48}$, $a_4 = a_3 \gamma'_{b,3}^{0.34}$, $\varepsilon_B = m_e c^2 B/B_{\text{cr}}$, $B_{\text{cr}} = 4.414 \times 10^{13}$ G, m_e is the electron rest mass.

The synchrotron spectrum emitted by electrons with power-law spectral index α , multiplied by the square of the photon energy, is given by

$$\frac{dN}{d\varepsilon' dt'} \varepsilon'^2 \approx \frac{2akU_B \varepsilon'^2}{\varepsilon_B^2} \left(\frac{2\varepsilon'}{\varepsilon_B} \right)^{-(\alpha+1)/2}, \quad (12)$$

and we use this formula for each power-law section of the electron spectrum.

The ICS part of the Eq. 7 cannot be obtained analytically in the general case because of the complicated form of the Klein-Nishina cross section, and so we compute this numerically using

$$\frac{dN}{dE'_\gamma dt'} E'^2_\gamma = E'^2_\gamma \int_{\gamma'_{\min}}^{\infty} \frac{dN}{d\gamma'} \int_{\varepsilon'_{\min}}^{\infty} \frac{dN(\gamma', E'_\gamma)}{dt' d\varepsilon' dE'_\gamma} d\varepsilon' d\gamma', \quad (13)$$

where $\gamma'_{\min} \approx E'_\gamma/m_e c^2$, $\varepsilon'_{\min} = E'_\gamma/[4\gamma'(\gamma' - E'_\gamma/m_e c^2)]$, $E'_\gamma = E_\gamma/D$, and $dN(\gamma', E'_\gamma)/dt' d\varepsilon' dE'_\gamma$ is the ICS spectrum (see Eq. 2.48, in Blumenthal & Gould 1970) produced by electrons with Lorentz factor γ' which scatter synchrotron photons in the blob, and we use in this formula the soft photon spectrum given by Eq. 4.

Having obtained formulae for the synchrotron power at 2 keV (Eq. 12) and the inverse Compton power at 1 TeV (Eq. 13), we can substitute these, together with the optical depth reduction factors, into the equation for η (Eq. 7). Setting $\eta = 3.6$, we solve this equation numerically to obtain B as a function of D for various values of t_{var} . The resulting allowed values of B versus D are plotted for $\xi = 1$ as the two thick full curves (for the low and high IRB models) in Figs. 3(a)–(c) for $t_{\text{var}} = 2.5$ hours, 20 minutes, and 2 minutes respectively. Fig. 3(d) is for $\xi = 1/3$ and $t_{\text{var}} = 2.5$ hours. In the next section we further constrain the allowed values of B and D by requiring the radiative time scales be consistent with the variability time scale.

4 Constraints from Radiative Time Scales

The simultaneous variability observed in TeV γ -rays and X-rays allow us to place a further constraint on the homogeneous SSC model. The observed decrease in the observed TeV γ -ray and X-ray fluxes may only occur if the electrons have sufficient time to cool during the flare,

$$t'_{\text{cool}} \leq t_{\text{var}} D. \quad (14)$$

This condition is required if the model is truly homogeneous, i.e. the model we consider in the present paper which includes a homogeneous magnetic field and constant jet direction and bulk Lorentz factor. In what follows, we consider the cooling time of electrons responsible for synchrotron radiation observed at 2 keV, i.e.

$$\gamma' = (2\varepsilon/D\varepsilon_B)^{1/2}, \quad (15)$$

with $\varepsilon = 2$ keV. The cooling time scale for synchrotron losses of electrons with Lorentz factor γ' is given by

$$t'_{\text{cool}}^{\text{syn}} = \frac{m_e c^2}{k U_B \gamma'}. \quad (16)$$

We next estimate the ICS cooling time. For the soft photon spectrum we adopt, some interactions with energetic electrons will be in the Thomson regime while others will be in the Klein-Nishina regime with relatively small energy loss. To calculate the cooling time, we neglect interactions in the Klein-Nishina regime, i.e. with photons above $\varepsilon'_T \approx m_e c^2/\gamma'$, and use the simple Thomson energy loss formula

$$t'_{\text{cool}}^{\text{ICS}} \approx \frac{m_e c^2}{k U_{\text{rad}}(< \varepsilon'_T) \gamma'}, \quad (17)$$

where

$$U_{\text{rad}}(< \varepsilon'_T) = \int_0^{\varepsilon'_T} n(\varepsilon') \varepsilon' d\varepsilon'. \quad (18)$$

Because the optical to X-ray energy flux per log energy interval, $F_E(E) \equiv E^2 F(E)$, increases with energy (i.e. the photon spectrum is flatter than ε^{-2}) most of the inverse Compton energy flux will occur near

$$E_\gamma \approx D\gamma'^2 \varepsilon'_T = D\gamma' m_e c^2. \quad (19)$$

Thus, the ratio of the energy loss times for inverse Compton and synchrotron loss for electrons with energies such that they radiate synchrotron photons which are observed with energies of $\varepsilon = 2$ keV is given by the ratio, ρ , of emitted energy flux per log energy

interval observed at $\varepsilon = 2$ keV to the emitted energy flux per log energy interval observed at a γ -ray energy of

$$E_\gamma \approx (2\varepsilon D/\varepsilon_B)^{1/2} m_e c^2, \quad (20)$$

where we have used Eqs. 15 and 19. The ratio is then

$$\frac{t'_{\text{cool}}^{\text{ICS}}(\gamma')}{t'_{\text{cool}}^{\text{syn}}(\gamma')} \approx \frac{F_E(\varepsilon)}{F_E(E_\gamma) \exp[\tau_{\text{tot}}(E'_\gamma)]} \equiv \rho(D, B, t_{\text{var}}, \xi). \quad (21)$$

Now, $E_\gamma = DE'_\gamma$ depends on D and B , and $\tau_{\text{tot}}(E'_\gamma)$ depends on D , t_{var} , ξ and B and the observed optical to X-ray SED, and so the ratio of emitted energy flux per log energy interval depends D , t_{var} , ξ , B and the observed SED.

The total blob-frame cooling time scale of electrons by both processes is given by

$$t'_{\text{cool}} = \left(\frac{1}{t'_{\text{cool}}^{\text{ICS}}} + \frac{1}{t'_{\text{cool}}^{\text{syn}}} \right)^{-1}, \quad (22)$$

and this must be less than the Doppler factor multiplied by the observed variability time,

$$\frac{1}{t'_{\text{cool}}^{\text{ICS}}} + \frac{1}{t'_{\text{cool}}^{\text{syn}}} > \frac{1}{Dt_{\text{var}}}. \quad (23)$$

Using $\rho(D, B, t_{\text{var}}, \xi)$ we can rewrite this in two separate ways in terms of the ICS and synchrotron cooling times in order to investigate which process dominates the electron cooling for specific parameters of the blob,

$$[1 + \rho(D, B, t_{\text{var}}, \xi)] Dt_{\text{var}} > t'_{\text{cool}}^{\text{ICS}}, \quad (24)$$

$$[1 + \rho(D, B, t_{\text{var}}, \xi)^{-1}] Dt_{\text{var}} > t'_{\text{cool}}^{\text{syn}}. \quad (25)$$

Each of the two equations above can be solved numerically for a given value of t_{var} to obtain a constraint on B as a function of D , and these two constraints have been added to Figs. 3(a)–(d). In each case, a separate curve is plotted corresponding to variability simultaneous with the TeV γ -rays occurring at 2 keV and 0.2 keV. In these figures the synchrotron cooling time scale of electrons is shorter than the observed variability time scale for parameters above the dot-dashed curves (given by Eq. 25), and the IC cooling time scale is shorter than the variability time scale for parameters to the left of the dotted curves (given by Eq. 24). Therefore, the parameter space allowed by the variability time scale condition (Eq. 23) lies above the dot-dashed curves to the left of the dotted curves.

Before discussing the implications of these new constraints we shall consider one further constraint. This constraint arises from the condition that the maximum energy of electrons (determined by the maximum energy of synchrotron photons) must be higher than the maximum energy of γ -ray photons in the blob frame, i.e.

$$\gamma'_{\text{max}} m_e c^2 > E_{\gamma, \text{max}} D^{-1}, \quad (26)$$

with $\gamma'_{\max} = (2\varepsilon_{s,\max}B_{\text{cr}}/m_e c^2 BD)^{1/2}$, and the maximum energy of synchrotron photon $\varepsilon_{s,\max}$. This condition gives an upper limit to the magnetic field in the blob

$$B < 4.4 \times 10^{-2} \varepsilon_{s,\max} D E_{\gamma,\max}^{-2} \text{ G}, \quad (27)$$

where $\varepsilon_{s,\max}$ is in keV and $E_{\gamma,\max}$ is in TeV. The low energy part of the spectrum from Mrk 501 extends up to at least 500 keV (Catanese et al. 1997) while the high energy part extends up to at least 24 TeV (Krawczynski et al. 1999, Konopelko et al. 1999). The constraint obtained using these values has been added to Figs. 3(a)–(d). In the next section we shall discuss the implications of the constraints obtained in this and the previous sections.

5 Discussion and Conclusion

We have now mapped out the allowed parameter space for $\xi = 1$ in Figs. 3(a)–(c) for $t_{\text{var}} = 2.5$ hours, 20 minutes, and 2 minutes respectively; Fig. 3(d) shows results for $\xi = 1/3$ and $t_{\text{var}} = 2.5$ hours. Allowed combinations of B and D lie on the thick solid curve corresponding to the infrared absorption model assumed (upper curve corresponds to lower IRB model). From the constraints on the inverse Compton and synchrotron cooling time scales, if the 2 keV X-ray flux is observed to vary during the flare with a similar time scale as the γ -rays, then allowed combinations of B and D must be to the left of the thick dotted curve labelled $t_{i,\text{I}}$, and above the thick dot-dashed curve labelled $t_{s,\text{I}}$. Similarly, if the 0.2 keV X-ray flux is observed to vary during the flare with a similar time scale as the γ -rays then allowed combinations of B and D must be to the left of the thin dotted curve labelled $t_{i,\text{II}}$ and above the thin dot-dashed curve labelled $t_{s,\text{II}}$. Finally, the requirement that a γ -ray energy be less than the energy of the electron producing it constrains the allowed combinations of B and D to be below the thick dashed curve.

Examining Figs. 3(a)–(c) we see that, as expected, as the variability time scale decreases, the Doppler factor and magnetic field required both increase, and the allowed range of $\log D$ and $\log B$ decrease somewhat. Comparing Fig. 3(d) for $\xi = 1/3$ with Fig. 3(a) for $\xi = 1$, both being for $t_{\text{var}} = 2.5$ hours, we see the effect of varying ξ is to increase the required magnetic field and to reduce the allowed range of $\log D$.

Not all of the parts of the thick solid curves within the “allowed” parameter space will actually give a viable SSC model as they may predict a high energy SED which may have a very different shape from that observed. To further delineate the allowed values of B and D we calculate the spectra of γ -rays emerging from the blob (after photon photon absorption in the blob synchrotron radiation) and propagating to Earth (through the infrared background). We have calculated the spectra for each of the points labelled A, B, C, or D, in Figs. 3(a)–(d) and normalized these to the observed flux at 1 TeV. The results are plotted for the lower IRB model in Figs. 4(a)–(d) respectively. Fig. 4(e) shows the result of using the upper IRB model (points labelled A', B', C', and D' in Fig. 3a) instead of the lower one, and we see that a worse fit to the observed spectrum results.

Table 1: Parameters for the best fits to the Mrk 501 spectrum.

Parameter	Spectrum	t_{var}	ξ	IRB model	B (G)	D
Fig. 3(a) C	Fig. 4(a)	2.5 hr	1	lower	0.1	11.5
Fig. 3(b) B	Fig. 4(b)	20 min	1	lower	0.2	20.4
Fig. 3(c) B	Fig. 4(c)	2 min	1	lower	0.6	35.5
Fig. 3(d) C	Fig. 4(d)	2.5 hr	1/3	lower	0.15	15.8
Fig. 3(a) C'	Fig. 4(e)	2.5 hr	1	upper	0.07	11.2

We now discuss which of these spectra are consistent with the observations. For the longest variability time scale considered, 2.5 hours (Figs. 4a, 4d and 4e), the parameters corresponding to the points labelled A and B are ruled out because of their poor agreement with the observed spectrum, and point C gives the best fit, with point D being acceptable provided further absorption (e.g. due to photons from the accretion disk, other parts of the jet, or a dusty molecular torus, Protheroe and Biermann 1997) can steepen the spectrum. As we go to shorter variability time scales (Figs. 4b and c) only points A are ruled out by the data. Table 1 summarizes the best-fitting model parameters for each case considered.

As seen in Fig. 3(d), which is for $t_{\text{var}} = 2.5$ hours and $\xi = 1/3$, the constraint from the IC cooling time scale and the observed variability at 0.2 keV is very close to ruling out the best-fitting spectrum (point C), and definitely rules out the spectrum corresponding to point D. It has been reported by Buckley and McEney (1999, cited by Catanese et al. 1997 and Kataoka et al. 1999) that U band observations show variability simultaneous with the TeV γ -rays. Such U band variability would further constrain the allowed values of D as the corresponding constraint from the IC cooling time scale would be significantly to the left of the curve labelled $t_{i,II}$ in Fig. 3(d), ruling out the best-fitting spectrum (point C). Inspection of Figs. 4(d) shows that spectra corresponding to points A and B in Fig. 3(d) are ruled out by their disagreement with observation. Thus, the reported U band observations would rule out all models with $\xi \leq 1/3$ implying that the allowed blob radius is larger than $\xi c D t_{\text{var}}/6$.

We would like to emphasize the importance of including photon-photon absorption in calculations when determining the allowed parameters of the SSC model. For example, in previous papers the energy at which the emitted energy flux per log energy interval maximizes in the γ -ray region is used when constructing constraints, as is the ratio of the peak luminosities. However, because of photon-photon absorption the energy at which the emitted energy flux per log energy interval maximizes can be significantly higher than the energy at which the observed energy flux per log energy interval maximizes, and this can lead to an incorrect determination of the allowed parameters. For example, we show in Fig. 5 that the maximum in the γ -ray spectrum shifts to lower energies by about an order of magnitude when photon-photon absorption is included; this has consequences for

the constraint obtained by Tavecchio et al. (1998) from a comparison of the location of the peaks in synchrotron and IC spectra.

Finally, we point out the importance of simultaneous multi-wavelength observations which are vital to properly determine the physical parameters of the emission region. To be most useful, these observations should cover the full energy ranges of both the low energy (synchrotron) and high energy (Compton) parts of the SED.

Acknowledgements

We would like to thank Anita Mücke for reading the manuscript and for helpful comments. W.B. thanks the Department of Physics and Mathematical Physics at the University of Adelaide for hospitality during his visit. This research is supported by a grant from the Australian Research Council and by the Polish Komitet Badań Naukowych grant 2P03D 001 14.

References

- Aharonian F. et al., 1997, *A&A*, 327, L5
Aharonian F. et al., 1998, *A&A*, 342, 69
Bednarek W., Protheroe R.J., 1997, *MNRAS*, 292, 646
Biller S. et al., 1998, *PRL*, 80, 2992
Bloom S.D., Marscher A.P., 1996, *ApJ* 461, 657
Blumenthal G.R., Gould R.J., 1970, *Rev. Mod. Phys.*, 42, 237
Catanese M. et al., 1997, *ApJ*, 487, L143
Catanese M. et al., 1998, *ApJ*, 501, 616
Chadwick P.M., et al., 1998, in *Proc. Veritas Workshop on the TeV Astrophysics of Extragalactic Objects*, in press
Djannati-Atai A. et al., 1998, *Abstracts of the 19th Texas Symposium on Relativistic Astrophysics and Cosmology*, held in Paris, France, Dec. 14-18, 1998. Eds.: J. Paul, T. Montmerle, and E. Aubourg (CEA Saclay).
Dondi, L., Ghisellini, G., 1995, *MNRAS*, 273, 583
Fixsen D.J., Dwek E., Mather J.C., Bennett C.L., and Shafer R.A., 1998, *ApJ*, 508, 123
Gaidos J.A. et al., 1996, *Nature*, 383, 319
Hauser M.G. et al., 1998, *ApJ*, 508, 44
Hayashida N. et al., 1998, *ApJ Lett.*, 504, L71
Inoue S., Takahara F., 1996, *ApJ* 463, 555
Jauch J.M., Rohrlich F., 1955, "The theory of photons and electrons", Addison-Wesley
Kataoka J. et al., 1999, *ApJ*, 514, 138
Konopelko A. et al., 1999, *Astropart.Phys.* submitted, astro-ph/990193
Krawczynski H. et al., 1999, in *Proc BL Lac Phenomenon Meeting*, Turku, ed. L. Takalo,

ASP Conference Series, in press
Krennrich F. et al., 1999, 511, 149
Macomb D.J. et al., 1995, ApJ, 449, L99 (Erratum 1996, ApJ 459, L111)
Malkan M.A., Stecker F.W., 1998, ApJ, 496, 13
Mastichiadis A., Kirk J.G., 1997, A&A, 320, 19
Mattox, J. R. et al., 1993, ApJ, 410, 609
Pian E. et al., 1998, ApJ, 492, L17
Protheroe R.J., Biermann P.L., 1997, Astropart. Phys., 6, 293
Protheroe R.J., Bhat C.L., Fleury P., Lorenz E., Teshima M., Weekes T.C., 1998,
in Proc. of 25th ICRC, Durban, Highlight Session on Mrk 501, M.S. Potgieter
et al. (eds.), 9, 317
Punch M. et al., 1992, Nature, 358, 477
Quinn J. et al., 1996, ApJ, 456, L83
Quinn J. et al., 1999, in preparation
Samuelson F.W. et al., 1998, ApJ, 501, L17
Stanev T., and Franceschini A., 1998, ApJ, 494, L159
Stecker F.W., and De Jager O.C., 1998, A&A, 334, L85
Svensson, R., 1987, MNRAS, 227, 403
Tavecchio F., Maraschi L., Ghisellini G., 1998, ApJ, 509, 608
Zweerink J. et al., 1997, ApJ, 490, L170

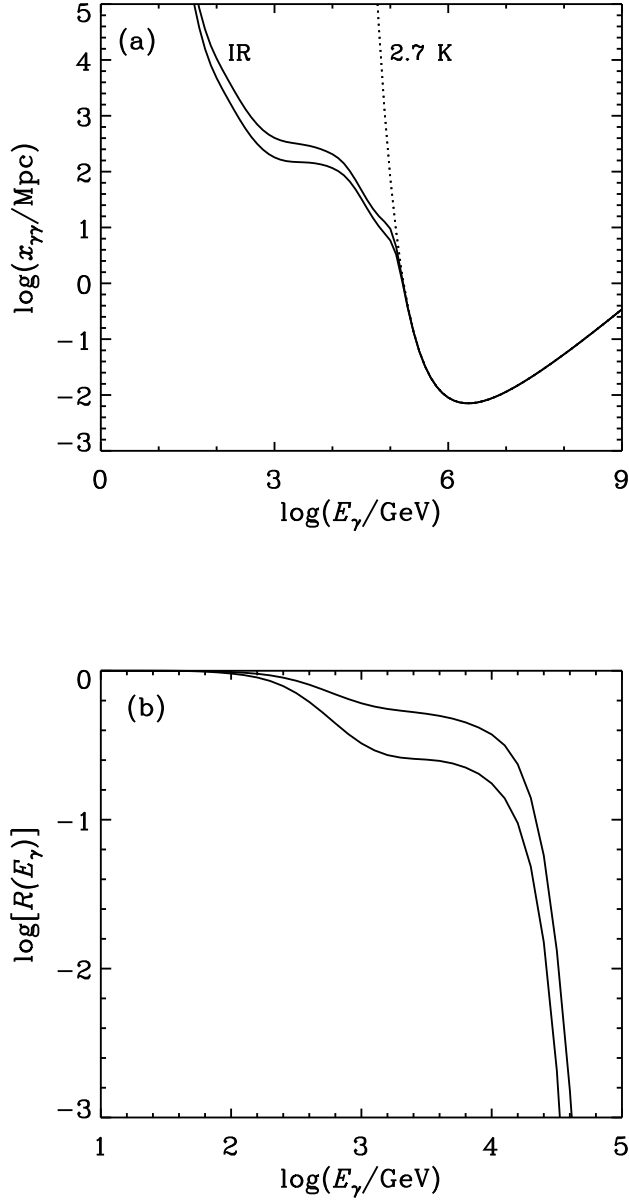


Figure 1: (a) Mean interaction length for photon-photon pair production in the cosmic microwave background plus infrared background upper and lower models of Malkan and Stecker (solid curves). Dotted curve labelled 2.7 K shows mean interaction length in the cosmic microwave background. (b) Reduction factor, $R(E_{\gamma}) = \exp(-\tau)$ for a source distance of 202 Mpc.

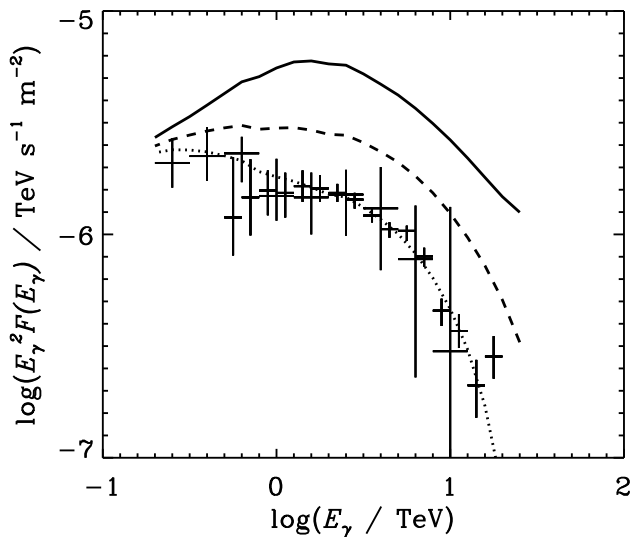


Figure 2: Mrk 501 1997 April 15–16 HEGRA data (data binned in 1/10 decade intervals) and CAT data (data binned in 1/5 decade intervals). The error bars on the HEGRA data include systematic errors as given in Fig. 1b of Krawczynski et al. (1999). The dotted curve shows the SED used in this paper, and the solid and dashed curves show the SED after correction for absorption using the lower and upper reduction factors of Fig. 1(b).

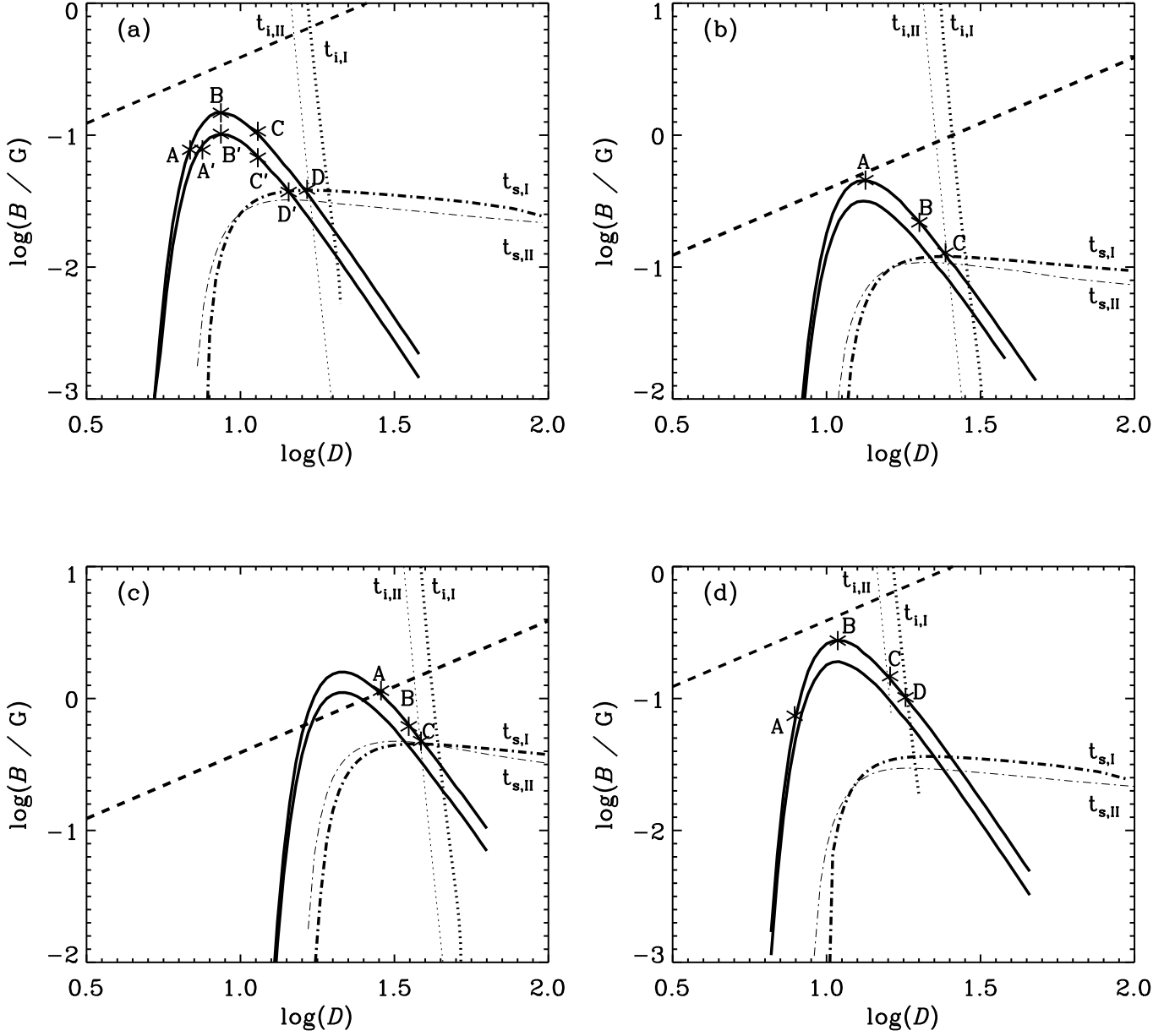


Figure 3: Constraints on the parameters (magnetic field B versus Doppler factor D) of the blob of assumed radius $0.5\xi ct_{\text{var}}D$ for the γ -ray flare on 15-16 April 1997 in Mrk 501 assuming different variability time scales of the flare: (a) $t_v = 2.5$ hr and $\xi = 1$, (b) $t_v = 20$ min and $\xi = 1$, (c) $t_v = 2$ min and $\xi = 1$, and (d) for $t_{\text{var}} = 2.5$ hr and $\xi = 1/3$. The full curves give the allowed values for B and D constrained by Eq. 7 for the case of absorption of γ -ray photons in the IRB using the lower model (upper curve) and the upper model (lower curve), the dot-dashed curves give the lower limit from the synchrotron cooling time scale (Eq. 25) and the dotted lines give the upper limit from the inverse Compton cooling time scale (Eq. 24) for electrons with energies which produce synchrotron photons with observed energies of 2 keV (thick lines marked by $t_{s,I}$ and $t_{i,I}$) and 0.2 keV (thin lines marked by $t_{s,II}$ and $t_{i,II}$), and the dashed curve gives an upper limit from the maximum energies of synchrotron and inverse Compton photons (Eq. 27). The points labelled A, B, etc., mark the values of B and D for which we have calculated γ -ray spectra and which we shall compare with observations in Fig. 4.

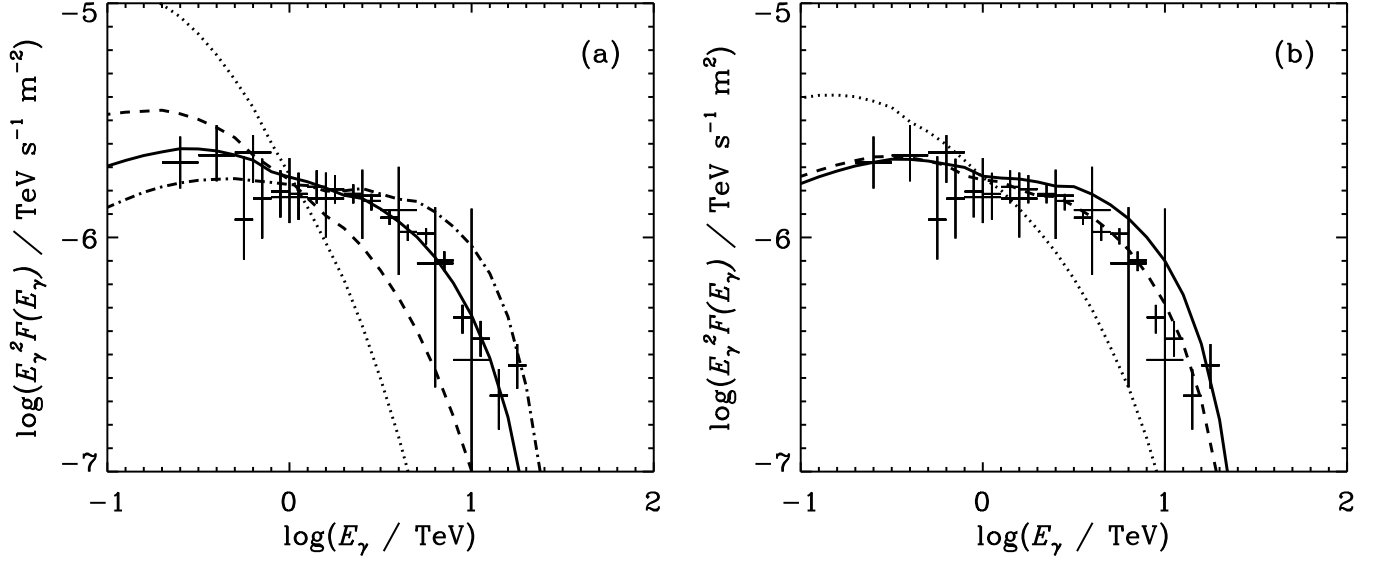


Figure 4: Gamma-ray spectra computed for the specific values of B and D using the lower IRB model are compared with the observations of Mrk 501 in the 15-16 April 1997 flare by the HEGRA (Krawczynski et al. 1999) and CAT (Djannati-Atai et al. 1998) telescopes: (a) $t_v = 2.5$ hr and $\xi = 1$, (b) $t_v = 20$ min and $\xi = 1$, (c) $t_v = 2$ min and $\xi = 1$, and (d) for $t_{\text{var}} = 2.5$ hr and $\xi = 1/3$. The spectra shown in (e) are obtained using the higher IRB model, $t_v = 2.5$ hr and $\xi = 1$. Specific spectra corresponding to different values of B and D indicated in Figs. 4(a)–(d) by A or A', B or B', C or C', and D or D' are shown by the dotted curves, dashed curves, solid curves, and dot-dashed curves, respectively.

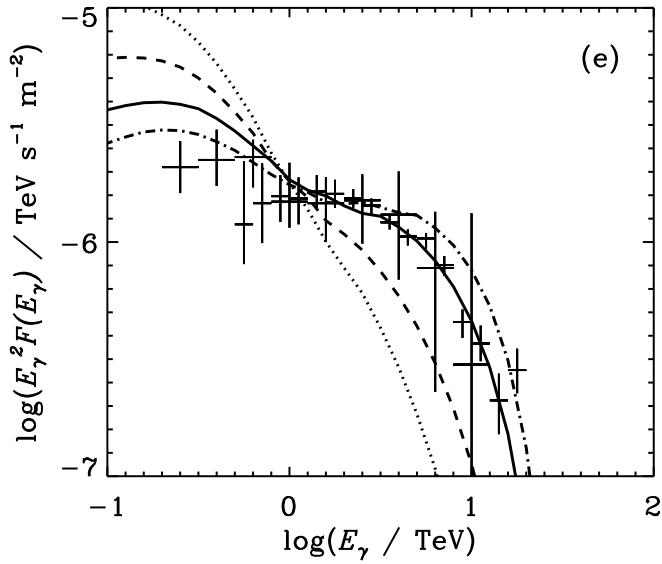
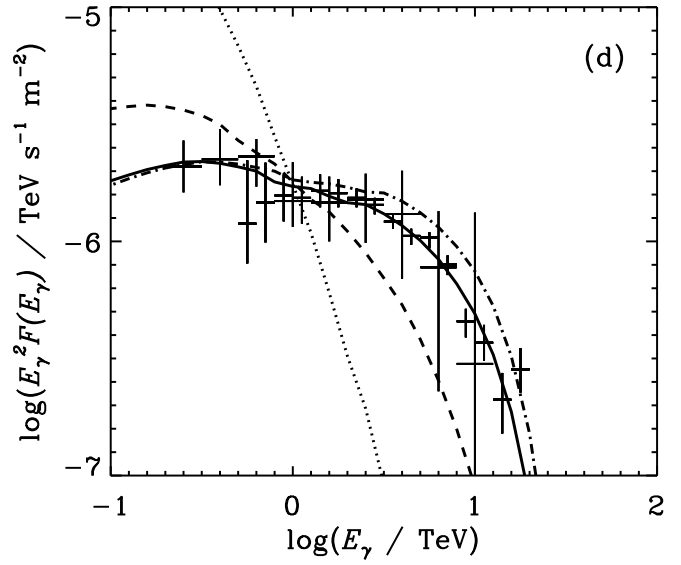
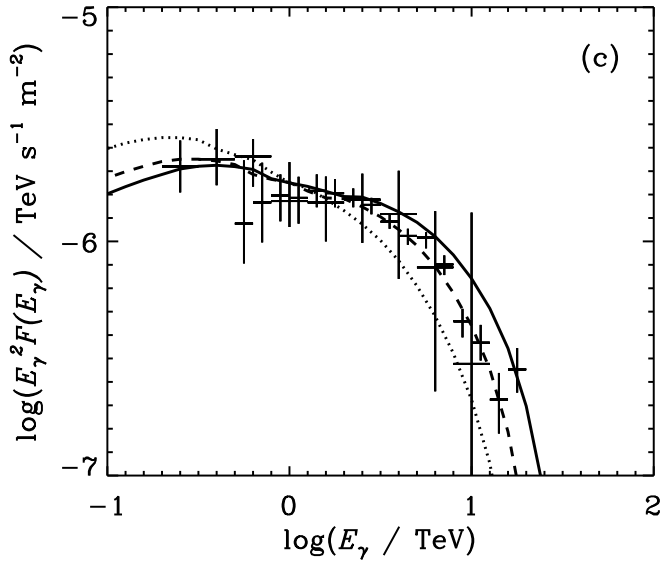


Figure 4: (Continued)

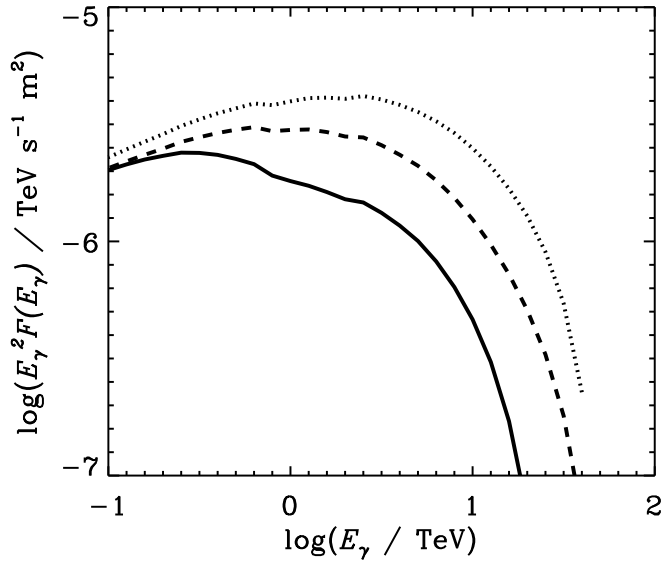


Figure 5: The γ -ray spectra computed for the parameters B and D given by the point C in Fig. 3a. The dotted curve shows the γ -ray spectrum produced in the blob by relativistic electrons. The dashed curve shows the γ -ray spectrum modified by absorption in the blob synchrotron radiation, i.e. the spectrum emerging from the blob. The full curve shows the γ -ray spectrum after propagation through the IRB using the lower IRB model.